JACS
JOURNAL OF THE AMERICAN CHEMICAL SOCIETY

Article

pubs.acs.org/JACS

Polymer-Fullerene Miscibility: A Metric for Screening New Materials for High-Performance Organic Solar Cells

Neil D. Treat,[†,‡] Alessandro Varotto,[§] Christopher J. Takacs,[∥] Nicolas Batara,[§] Mohammed Al-Hashimi,[⊥] Martin J. Heeney,[⊥] Alan J. Heeger,[†,‡,§,∥] Fred Wudl,[†,‡,§] Craig J. Hawker,[†,‡,§] and Michael L. Chabinyc*[,†,‡]

[†]Materials Department, [‡]Materials Research Laboratory, [§]Department of Chemistry and Biochemistry, [∥]Department of Physics, University of California Santa Barbara, Santa Barbara, California 93106, United States

[⊥]Department of Chemistry and Centre for Plastic Electronics, Imperial College, London, SW7 2AZ, United Kingdom

Supporting Information

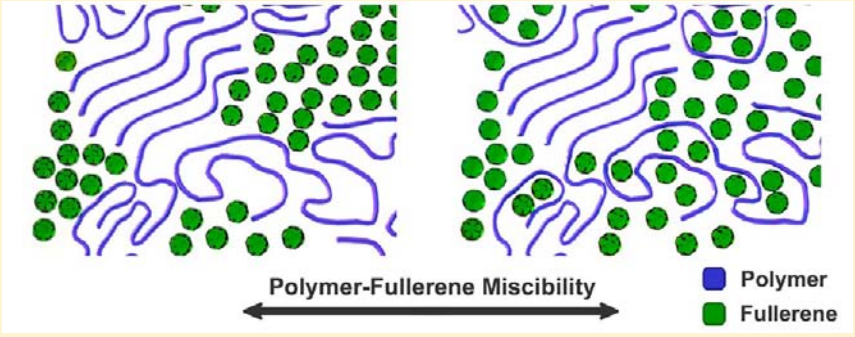

ABSTRACT: The improvement of the power conversion efficiency (PCE) of polymer bulk heterojunction (BHJ) solar cells has generally been achieved through synthetic design to control frontier molecular orbital energies and molecular ordering of the electron-donating polymer. An alternate approach to control the PCE of a BHJ is to tune the miscibility of the fullerene and a semiconducting polymer by varying the structure of the fullerene. The miscibility of a series of 1,4-fullerene adducts in the semiconducting polymer, poly(3-hexylselenophene), P3HS, was measured by dynamic secondary ion mass spectrometry using a model bilayer structure. The microstructure of the bilayer was investigated using high-angle annular dark-field scanning transmission microscopy and linked to the polymer-fullerene miscibility. Finally, P3HS:fullerene BHJ solar cells were fabricated from each fullerene derivative, enabling the correlation of the active layer microstructure to the charge collection efficiency and resulting PCE of each system. The volume fraction of polymer-rich, fullerene-rich, and polymer-fullerene mixed domains can be tuned using the miscibility leading to improvement in the charge collection efficiency and PCE in P3HS:fullerene BHJ solar cells. These results suggest a rational approach to the design of fullerenes for improved BHJ solar cells.

INTRODUCTION

Organic photovoltaics (OPVs) offer great potential as a low-cost thin film solar cell technology due to their ability to be solution processed over large areas. The last four years have yielded a tremendous improvement in the power conversion efficiency (PCE) of bulk heterojunction (BHJ) OPVs, from 5.15% to over 10%.[1,2] This improvement in PCE can be linked to the design of new semiconducting materials (improvement in the overlap of absorbance with the solar spectrum)[3−8] and to the control of the active layer microstructure through processing (addition of high boiling point solvents).[9−11] However, our inability to predictably control the microstructure within BHJ blends, and thus their PCE illustrates a lack of knowledge concerning the factors that control the active layer microstructure (i.e., volume fraction of polymer- and fullerene-rich and mixed domains). This lack of understanding limits the optimization of new electron-donating and -accepting materials in solar cells to trial-and-error approaches. Therefore, it is critically important to develop knowledge and associated strategies for controlling the equilibrium microstructure of BHJ organic solar cells.

The most efficient polymer-fullerene BHJ active layers contain a multiphase blend of an electron-donating polymer and electron-accepting fullerene derivative. Many independent studies have demonstrated that polymer-fullerene BHJs comprise a combination of pure polymer, pure fullerene, and mixtures of the disordered polymer and fullerene components.[12−20] The PCE of this system is therefore intimately linked to the active layer morphology and the relationship between these three phases. For example, photoexcited states in the electron-donating polymer component must be in close proximity (i.e., exciton diffusion length) to an electron-accepting fullerene derivative in order to generate mobile charge carriers, which have a greater probability of occurring within the highly mixed polymer- and fullerene-rich domains.

Received: June 17, 2012
Published: September 13, 2012

These mobile charge carriers must then escape to either electrode, which is aided by the polymer- and fullerene-rich domains. As a result, tuning the volume fraction of the rich to intermixed phases will strongly influence the photoexcited state dissociation and the free charge carrier collection efficiency and thereby the PCE.

With few exceptions, the recent remarkable improvement in the PCE of polymer-fullerene BHJs is linked to the development of new electron-donating polymers with improved optical and electronic properties.[21] Generally, the maximum experimentally achievable PCE for a new class of semiconducting polymers is determined by forming BHJs with a single derivative of electron-accepting fullerene, e.g., [6,6]-phenyl-C_{61}-butyric acid methyl ester (PCBM) or $PC_{70}BM$.[3,4,21−25] In addition to the backbone structure of the donor polymer, the side chain structure has been demonstrated as a means to modify the PCE most likely through modification of the microstructure of the blend.[6,26−30] Interestingly, many novel semiconducting polymers have been synthesized with near ideal molecular orbital energies that should facilitate both charge transfer and light absorption but do not achieve their maximum efficiency when blended with PCBM.[3,31] The lower performance is often attributed to an unoptimized morphology, but in many cases, it is not clear how to change the microstructure to increase the PCE.

Tuning the fullerene architecture is a potentially elegant solution for controlling the microstructure and PCE of polymer-fullerene BHJs.[32−34] Through complementary techniques, recent investigations have found the fullerene, usually $PC_{60}BM$ or $PC_{70}BM$, is disordered and rapidly diffuses in most efficient BHJ devices.[12,15] In direct contrast to the polymer case, it has been found in many cases that significant changes to the structure of the fullerene component have a minimal effect on the PCE.[13,32,35−40] To determine if this is a general trend for fullerene derivatives, it is necessary to determine how the nature of the fullerene derivatives influence the polymer-fullerene miscibility, active layer microstructure, and resulting PCE.

In this report, we systematically tune the fullerene structure for a series of novel 1,4-diadducts and link these changes to the polymer-fullerene miscibility and to the active layer microstructure and resulting PCE. For these studies, we examined an electron-donating polymer, regioregular poly(3-hexyl selenophene) (P3HS) which is structurally similar to the widely studied P3HT but with a lower bandgap. P3HS:PCBM BHJ devices have been previously shown to suffer from low PCE and poor free charge carrier collection, which was attributed to the high miscibility between P3HS and PCBM leading to inefficient electron collection pathways.[41] To reduce the miscibility of the fullerene in P3HS, a series of 1,4-fullerene adducts was utilized with different alkoxy chain lengths.[36] The miscibility of these fullerene derivatives in P3HS was quantified by investigating the interdiffusion of a P3HS/fullerene bilayer using dynamic secondary ion mass spectrometry (DSIMS). It was found that the temperature-dependent polymer-fullerene miscibility increased with increasing fullerene alkyl chain length. High-angle annular dark field (HAADF) scanning transmission electron microscopy (STEM) images of the annealed bilayer films also indicate that the volume fraction of polymer- and fullerene-rich domains increases as the polymer-fullerene miscibility was reduced. Additionally, a combination of HAADF-STEM and high-resolution transmission electron microscopy (HR-TEM) demonstrated that the microstructures of P3HS/fullerene bilayer samples were analogous to the BHJ microstructure, thus further validating the miscibilities measured with the bilayer structures. Finally, the fabrication of P3HS:fullerene BHJ solar cells shows that reducing the miscibility of the fullerene in P3HS improves the charge collection efficiency and decreases bimolecular recombination, which improves the PCE. This study demonstrates that the polymer-fullerene miscibility can be used to systematically tune the volume fraction of polymer- and fullerene-rich and polymer-fullerene mixed domains, which ultimately improves the charge collection efficiency and PCE of organic BHJ solar cells.

EXPERIMENTAL SECTION

Materials. Poly(3-hexylthiophene) (Sepiolid P200) and [6,6]-phenyl-C_{61}-butyric acid methyl ester (99.5%) were used as received from BASF and Nano-C, respectively. Poly(3-hexyl)selenophene was synthesized by the reported procedure (ref 46) to afford a polymer with M_w of 74 000 g/mol, a polydispersity index of 1.27, and a regioregularity of 96% based upon ^{1}H NMR integration of the methylene region.

Synthesis and Characterization. 1-(1,2,3-(trihexyloxy)benzene-4-phenyl-1,4-dihydro[60]fullerene ($(C_6H_{13})_3$-OBP or PTHOB) was synthesized as prior reported.[36] Deuterated 1,4 addends were synthesized according to the same procedure described above using deuterated phenylhydrazine hydrochloride (deuterated phenylhydrazine was synthesized according to the literature).[42]

^{1}H NMR (500 MHz, $CDCl_3$) δ ppm 0.94 (m, 10H), 1.39 (m, 14H), 1.70 (m, 2H), 1.8 (s, 4H), 4.08 (m, 4H), 4.25 (m, 2 H), 6.78 (d, 1H), 7.43 (m, 1H), 7.47 (m, 2H), 7.81 (d, 1H), 8.09 (d, 2H). ^{13}C NMR (600 MHz, $CDCl_3$) δ ppm 14.03, 14.10, 22.58, 22.58, 22.67, 22.71, 25.60, 25.88, 29.39, 29.91, 31.67, 31.72, 31.85, 59.61, 61.72, 68.90, 73.80 (sp_3-C of C_{60}), 74.36 (sp_3-C of C_{60}), 108.21, 124.20, 126.52, 127.70, 128.03, 129.26, 137.96, 137.99, 138.80, 138.96, 140.89, 141.82, 142.20 142.30, 142.45, 142.67, 142.82, 142.86, 143.06, 143.21, 143.26, 143.28, 143.43, 143.63, 143.84, 143.92, 144.03, 144.10, 144.24, 144.39, 144.42, 144.46, 144.49, 144.56, 144.65, 144.67, 144.91, 145.02, 145.05, 145.22, 145.26, 145.57, 145.61, 145.67, 145.90, 146.87, 146.92, 147.14, 147.20, 147.48, 147.62, 148.20, 148.73, 148.89, 150.79, 151.57, 152.53, 153.91, 156.33, 156.98. FD 1175 amu. UV−vis (1,2-dichlorobenzene) λ_{max}/nm 334, 446, 540, 620, 690.

1-(1,2,3-(tripropyloxy)benzene-4-phenyl-1,4-dihydro[60]fullerene ($(C_3H_7)_3$-OBP or PTPOB). The synthesis of PTPOB is analogous to PTHOB using 1,2,3-propyloxybenzene in place of hexyloxybenzene.

1-(1,2,3-(triethyloxy)benzene-4-phenyl-1,4-dihydro[60]fullerene ($(C_2H_5)_3$-OBP or PTEOB). The synthesis of PTEOB is analogous to PTHOB using 1,2,3-ethylyloxybenzene in place of hexyloxybenzene.

Quantifying Fullerene Miscibility. Thermally grown silicon oxide (150 nm thick) on silicon substrates was cleaned in an ultrasonic bath with acetone, 2% soap in water, deionized water, and 2-propanol for 20 min each, dried with N_2, and transferred into a N_2-filled glovebox for spin coating. P3HS and *d*-fullerene (15 and 45 mg/mL in chlorobenzene, respectively) solutions were then deposited via spin coating at 1200 rpm for 40 s and allowed to age in an inert environment for 2 days prior to bilayer fabrication. To fabricate the bilayers, the films of P3HS on SiO_2/Si substrates were immersed in 5% vol HF solution in water followed by careful immersion in deionized water yielding a film of P3HS floating on a water support. Then, *d*-fullerene films on SiO_2/Si were used to pick up the floating polymer films and dried in vacuum (10 mbar) for 30 min to ensure proper film formation. Samples were then thermally annealed in a N_2-filled glovebox on a preheated hot plate (which had been calibrated with an IR thermometer and thermal probe) for various temperatures and times and were cooled placing on a room temperature metal surface. Finally, a 70 nm thick polystyrene (150 kDa GPC standard) film was prepared by spin coating at 1200 rpm from a 15 mg/mL solution in toluene on a SiO_2/Si substrate and floated on a DI H_2O surface by sequential immersion in 5% vol HF and DI H_2O. The P3HS/*d*-

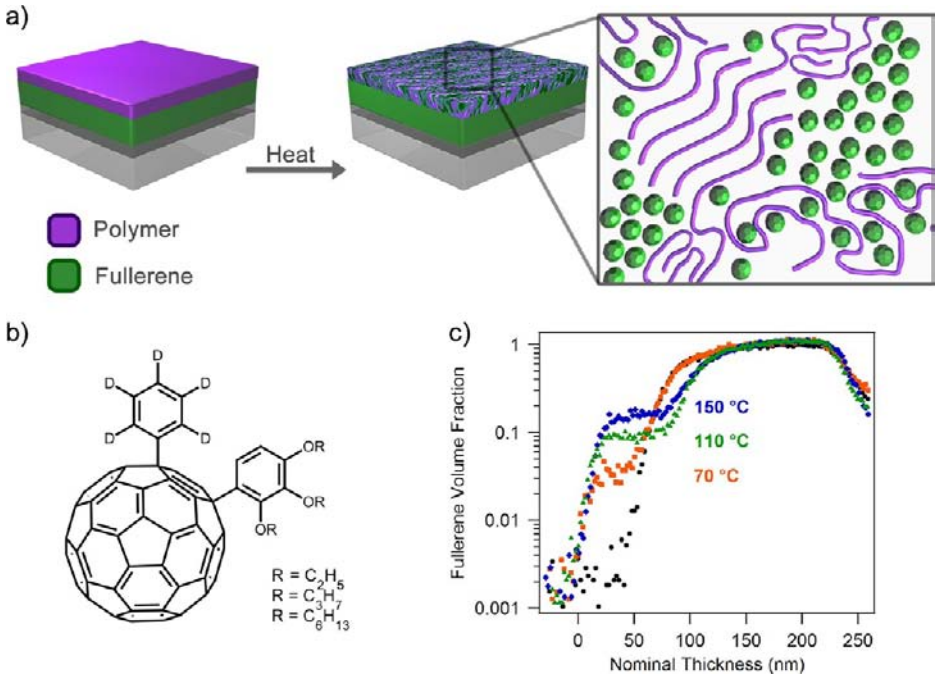

Figure 1. (a) Schematic representation of an (left) as prepared and (right) annealed P3HS/*d*-fullerene bilayer films fabricated on SiO_2/Si. The inset represents the microstructure of the polymer-fullerene film comprised of ordered and disordered polymer domains, disordered fullerene domains, and mixed polymer-fullerene domains present in the bilayer after annealing. (b) Chemical structure of the 1,4-fullerene adduct with varying lengths of alkyloxy side chains. (c) DSIMS profiles of the ^2H signal in a P3HS/$(C_3H_7)_3$-OBP bilayer sample annealed for 10 min at various temperatures. The ^2H signal in the pure *d*-fullerene film is normalized to 1 and plotted against the nominal thickness of the bilayer film.

fullerene/SiO_2/Si substrate was then used to lift the PS film from the water. This layer was used as a capping layer to ensure the stabilization of the O_2^+ beam before analysis of the sample of interest. The final film structure consisted of PS/P3HS/*d*-fullerene/SiO_2/Si. We note that all fullerene derivatives used have five ^2H atoms per molecule, which allows their concentrations to be directly compared.

Solar Cell Fabrication and Characterization. ITO-coated glass substrates were ultrasonicated in acetone, 2% soap in water, deionized water, and 2-propanol for 20 min and dried with nitrogen. A 40 nm thick film of PEDOT:PSS (Clevios PVP Al 4083) was deposited by spin coating at 4000 rpm for 40 s and dried at 165 °C for 10 min. The P3HS and fullerene stock solutions were prepared in chlorobenzene in a N_2 glovebox at a concentration of 20 and 30 mg/mL, respectively, stirred overnight at 80 °C, and filtered with a 0.45 μm PTFE filter prior to use. All devices were fabricated so that the molar ratio of polymer to fullerene was equal to a weight ratio for P3HT:PCBM of 1:0.7 with 1.5% vol 1-chloronaphthalene; the total solution concentration was modulated so that an active layer thickness of ~90 nm was maintained, nominally 20 mg/mL based on total solids. These solutions were spin coated at 800 rpm for 40 s and then at 2000 rpm for 5 s on the prepared substrates. The electrodes were then evaporated under vacuum ($<10^{-6}$ Torr). Lithium fluoride was typically evaporated at a rate of ~0.15 Å/s for a final thickness of 1.5 nm. Aluminum was typically evaporated at a rate of ~3 Å/s with a final thickness of >75 nm. Each substrate contained 5 solar cells each having an area of 0.06 cm^2.

The *J*−*V* characteristics were measured at 1 sun (AM 1.5G) in a N_2-filled glovebox equipped with a Xenon lamp (Newport) and Keithley 2408 SMU. EQE spectra were collected in a N_2-filled glovebox equipped with a 300 W Xe source, a McPherson EU-700-56 monochromator, and optical chopper and lock-in amplifier with a National Institute of Standards and Technology traceable silicon photodiode for monochromatic power−density calibration. The light intensity dependent *J*−*V* curves were measured with an array of 14 red 1W LEDs in a N_2-filled glovebox. The devices were measured in a light then dark sequences using a Keithley 2400 source meter unit.

TEM Characterization. Samples were prepared using SiO_2/Si substrates in the same manner as solar cells or bilayer samples. After thermal treatment, the underlying SiO_2 layer was etched in dilute HF, and the samples were floated onto the DI water/air interface. The films were transferred to C-Flat TEM grids with 2 μm holes. Before transfer of the film, 15 nm citrate stabilized gold nanoparticles were deposited on the grids to aid with focusing of the beam in STEM and HRTEM modes. The solution was allowed to sit for 5 min, and then the grids were washed with isopropyl alcohol to prevent aggregation of the particles. TEM characterization was performed on a FEI Titan microscope operating at 300 kV. STEM was performed using a probe convergence angle of 10 mrad. The annular detector distance was 160 or 196 mm for the films shown in the main text and 102 mm for the images contained in the Supporting Information. In all cases, the contrast should be approximately proportional to Z^2. HRTEM images were acquired using low-dose imaging technique described in Sun et al.[43]

■ RESULTS AND DISSCUSSION

P3HS is an ideal candidate to investigate the effects of polymer-fullerene miscibility on the active layer morphology and photoconversion efficiency. P3HS is structurally identical to P3HT except for the substitution of the selenium heteroatom for a sulfur heteroatom and has a similar crystalline packing structure.[44−46] This substitution leads to a reduction in the optical band gap for P3HS (E_g = 1.6 eV) compared to P3HT (E_g = 1.9 eV), and one would expect a ~55% increase in the short circuit current density (J_{sc}) for an ideal solar cell under 1 sun illumination (assuming that all available photons are converted to charge and collected). The molecular order of the two polymers has also been found to be similar (e.g., similar molecular packing),[44−46] but surprisingly, the maximum reported peak quantum efficiency for P3HS:PCBM solar cells is less than half of that achieved by P3HT:PCBM solar cells: ~38% vs ~77%. Importantly, the fill factor (FF) in

dx.doi.org/10.1021/ja305875u | J. Am. Chem. Soc. 2012, 134, 15869−15879

P3HS:PCBM devices was observed to be much lower for the corresponding P3HT:PCBM devices, 44% vs 71% (Figure S1a), respectively. This corresponds to a higher probability for recombination (or worse charge collection efficiency) in the P3HS:PCBM solar cells evidenced by less efficient charge transport in transient photovoltage measurements.[41]

The inefficiency of P3HS:PCBM BHJs is due to their microstructure. By using Raman scattering cross sections, it was concluded that the decreased charge collection efficiency was due to a significantly increased degree of miscibility between P3HS and PCBM relative to P3HT and PCBM.[41] Here we measured the miscibility of PCBM in P3HS via DSIMS diffusion couple experiments (Figure S1b) and determined that PCBM is at least 65% more miscible in P3HS relative to P3HT at 110 and 150 °C. These findings suggest that the poor charge collection efficiency is due to an inadequate volume fraction of fullerene-rich domains due to the miscibility of PCBM in P3HS. As a consequence, inefficient charge collection is observed.

To improve the PCE of P3HS:fullerene BHJs solar cells, an alternative fullerene to PCBM must be chosen. Here we demonstrate a methodology to rationally improve the performance of BHJ of P3HS. By specifically tailoring a series of fullerene derivatives, we aim to develop a fundamental understanding of structure/property relationships in bulk heterojunction systems and demonstrate how decreasing the miscibility of the fullerene component in P3HS will increase the volume fraction of fullerene-rich domains and improve the collection of free charge carriers and the PCE.

Quantification of Polymer-Fullerene Miscibility. In the P3HS:fullerene BHJ, increasing the volume fraction of fullerene-rich domains is expected to improve charge carrier collection; thus decreasing the miscibility of the fullerene component in the polymer phase is a reasonable strategy. To systematically vary the miscibility of the fullerene and polymer, a series of 1,4-fullerene diadducts with different lengths of alkyloxy chains were synthesized, which allowed for the tuning of the miscibility without influencing the optical and electronic properties of the fullerene [i.e., frontier molecular orbitals from CV (Figure S9)]. These fullerenes are denoted as $(C_2H_5)_3$-OBP, $(C_3H_7)_3$-OBP, and $(C_6H_{13})_3$-OBP for the triethyloxy, tripropyloxy, and trihexyloxy modified derivatives (chemical structure in Figure 1b and synthesis details are described in the experimental and literature).[36]

P3HS/*d*-fullerene bilayers on SiO_2/Si substrates were fabricated using a float-casting technique to quantify the polymer-fullerene miscibility. Films of P3HS and *d*-fullerene films were separately spin cast with thicknesses of 60 and 180 nm, respectively, and aged in an inert environment for 2 days prior to further processing. The P3HS film was then floated onto a deionized water surface and picked up by the supported fullerene film forming a pure bilayer of P3HS/fullerene on a SiO_2/Si substrate (Figure 1a left). The vertical concentration profiles of the P3HS/fullerene bilayer samples were investigated using DSIMS. ^{2}H labeled fullerenes were used due to the high specificity when examining with DSIMS (additional data presented in the Supporting Information). The as-prepared bilayer sample (Figure 1c, black circles) shows two distinct layers within the sample: a ^{2}H-deficient polymer layer and a ^{2}H-rich *d*-fullerene layer. The ^{2}H signal within the polymer layer corresponds to the natural abundance of deuterium (0.015% of ^{1}H) signifying a pure P3HS layer. The width of the interface between the P3HS and *d*-fullerene layers is ~20 nm, which is near the depth resolution of the DSIMS (~10 nm).

The P3HS/*d*-fullerene bilayer samples were heated at 70, 110, and 150 °C for 10 min and the vertical concentration profile of the *d*-fullerene in the P3HS was measured using DSIMS. Similar to previous studies,[12] the concentration of the fullerene (for all derivatives) found in the P3HS layer increased with increasing temperature (Figure 1c). All fullerene derivatives were found to have a uniform concentration profile within the P3HS layer. This indicates that the diffusion coefficient must be greater than 10^{-10} cm^2/s as was concluded with other systems.[12,14] Additionally, the fullerene concentration profile in the polymer remained unchanged at annealing times longer than seconds, which indicates the concentration of fullerene measured in polymer layer is the fullerene miscibility in the amorphous portion of the polymer. This fraction of miscible fullerene is dispersed with the disordered P3HS domains at elevated temperature (as depicted in Figure 1a, Figure S7). Upon cooling to room temperature, a portion of the miscible fullerene fraction aggregates into fullerene-rich domains (<200 nm in size as observed in the HAADF-STEM below). It is important to note that values for the polymer-fullerene miscibility reported in this study are determined from the total volume of miscible fullerene (at elevated temperature) within the area ablated during the DSIMS measurement (~300 × 300 μm). However, it is understood that the fullerene derivatives are not miscible with the ordered domains of the semicrystalline polymer layer. Thus, this treatment yields a conservative estimate for the volume fraction of fullerene miscible in the disordered polymer domains, and the values for the polymer-fullerene miscibility reported in this study are based on the total volume of the fullerene in a P3HS layer after annealing.

The volume fraction of miscible *d*-fullerene in P3HS increased as a function of annealing temperature and alkyl chain length of the OBP. Figure 2 plots the volume fraction of fullerene miscible in the polymer layer (as described above) as a function of annealing temperature. As the length of the pendant alkyl chains was increased from ethyl to hexyl, the amount of fullerene miscible in the polymer layer increased by a factor of ~15 (φ_{C2H5} = 0.05, φ_{C3H7} = 0.14, φ_{C6H13} = 0.68, φ_{PCBM} = 0.73 measured at 150 °C). These values for the polymer-fullerene miscibility correspond to the volume fraction of "dissolved" fullerene in the polymer film at the annealing temperature.

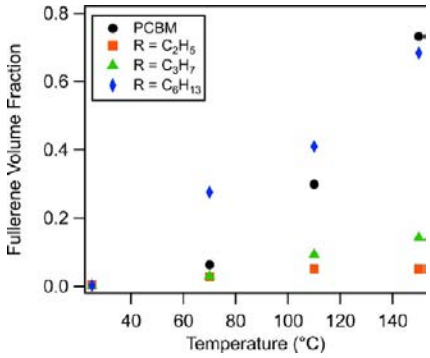

Figure 2. Plot of the volume fraction of *d*-PCBM (black circles), $(C_2H_5)_3$-OBP (orange squares), $(C_3H_7)_3$-OBP (green triangles), or $(C_6H_{13})_3$-OBP (blue diamonds) in the P3HS layer of a P3HS/d^5-fullerene bilayer sample annealed at 70, 110, and 150 °C for 10 min.

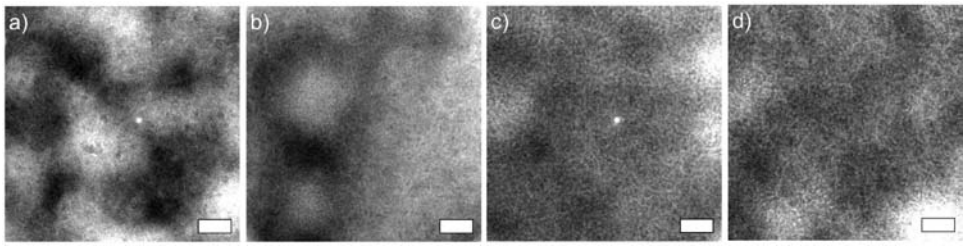

Figure 3. HAADF STEM of: (a) P3HS/$(C_2H_5)_3$-OBP, (b) P3HS/$(C_3H_7)_3$-OBP, (c) P3HS/$(C_6H_{13})_3$-OBP, and (d) P3HS/PCBM bilayer samples annealed at 150 °C for 10 min. The bright spot in (a,c) is an artifact from focusing the beam prior to imaging. The intensity scale is ±37.5% of the mean value, and the scale bar is 200 nm.

Significantly, control over the polymer-fullerene miscibility was achieved without affecting the frontier molecular orbital energy levels and the optical properties of the fullerene, material properties that are of utmost importance for the correlation of the active layer microstructure to the PCE. Therefore, these findings illustrate that decreasing the alkyl chain length of the 1,4-fullerene adducts decreases the polymer-fullerene miscibility at all temperatures.

Linking the Polymer-Fullerene Miscibility to the Bilayer Microstructure. The polymer-fullerene miscibility was linked to the microstructure (i.e., the ratio of polymer- and fullerene-rich and polymer-fullerene mixed domains) of the polymer layer in a P3HT/fullerene bilayer film after annealing at 150 °C for 10 min. The role of miscibility on the microstructure of the annealed bilayer samples was investigated using HAADF STEM. HAADF STEM is particularly sensitive to the atomic number, Z, and has previously been used to investigate the morphology of P3HS:PCBM blends.[47,48] To form an image, the electron beam is focused to a point, rastered across the sample, and electrons scattered to high angles are collected by an annular detector. At these high angles, the scattered intensity scales as Z^2; thus each selenium heteroatom in P3HS contributes the equivalent signal as 25 carbon atoms, compared to the sulfur atom in P3HT where it is only 7 carbon atoms.[49,50] The remaining monomer contains 10 carbon atoms, and the contribution from the hydrogen atoms can be neglected. The selenium atom alone will be responsible for ∼70% of the collected scattering in P3HS. Thus, the total scattering of P3HS is about twice that of P3HT and well-beyond that of the fullerene per unit volume. This inverts the contrast commonly observed in BHJ images and dramatically increases the contrast between components. Accordingly, the brighter areas correspond to polymer-rich phases, while the darker areas correspond to fullerene-rich phases.

Studying the bilayer samples at room temperature after heating to 150 °C enables the quantification of the final structure of the miscible fraction of fullerene in the polymer without complications that arise from the more complicated codeposition process. The HAADF STEM images for P3HS/$(C_2H_5)_3$-OBP, $(C_3H_7)_3$-OBP, $(C_6H_{13})_3$-OBP, and PCBM bilayer films annealed at 150 °C for 10 min are presented in Figure 3a−d, respectively.

Not surprisingly, decreasing the fullerene miscibility in P3HS results in an increase in the volume fraction of fullerene-rich domains as indicated by the increase in heterogeneity. We emphasize that STEM is a projection measurement, for a true bilayer of smooth films, one would not expect to observe micro- or nanostructure. With annealing, the miscible fraction of fullerene diffuses into the polymer layer resulting in a microstructure comprising pure polymer crystallites and highly intermixed polymer and fullerene domains. Upon cooling, these highly mixed polymer and fullerene domains self-assemble to form a percolated structure, where the final structure is governed by the polymer-fullerene miscibility. These top-down projection images of bilayers were similar to those from conventional BHJ samples. In these bilayer samples, both a discernible micro- and nanostructure develop after thermal annealing and cooling to room temperature. All samples show some degree of large-scale structures, approaching a length scale of micrometers, presumably due to thickness fluctuations of the samples and some large-scale aggregation of the phases. For the bilayer with $(C_2H_5)_3$-OBP, the least miscible of the series, we observe crystallites of the fullerene, i.e., the large, discontinuous structure, with no discernible nanostructure from intermixing (ordered fullerene confirmed by XRD, Figure S7). The $(C_3H_7)_3$-OBP, while not showing any degree of fullerene crystallinity, shows some deviations from a uniform background on length scales of 20−50 nm, indicating intermixing, and the formation of percolated structures within the blend film. Finally, the $(C_6H_{13})_3$-OBP and PCBM bilayer films show similar microstructures relative to the $(C_3H_7)_3$-OBP derivative, but the fluctuations appear more dramatic/intense, indicating a more developed nanomorphology. Considered together, these imaging results reveal that even with subtle changes in the fullerene structure it is possible to tune the miscibility and nanostructure. It was interesting to note that the bilayer films made from both $(C_6H_{13})_3$-OBP and PCBM, fullerenes with dissimilar chemical structures but similar miscibilities, exhibited qualitatively similar nanomorphology. Importantly, these data indicate that fullerene derivatives with dissimilar structures but similar polymer-fullerene miscibilities can yield BHJs with comparable microstructures. Thus, polymer-fullerene miscibility is a demonstrably important material property, which governs the formation of the charge collection pathways within BHJ solar cells.

Linking the Polymer-Fullerene Miscibility to the BHJ Microstructure. The BHJ active layer morphology was characterized using a combination of HAADF STEM and HR-TEM enabling the correlation of the polymer-fullerene miscibility to the BHJ active layer microstructure and ultimately the PCE of the BHJ solar cell. A number of morphological features in the micro- and nanostructure of the bilayer films are observed in the codeposited BHJ films. Figure 4a,b shows HAADF STEM images of P3HS:fullerene BHJ active layers with $(C_3H_7)_3$-OBP and $(C_6H_{13})_3$-OBP after annealing at 150 °C for 10 min. The P3HS:$(C_3H_7)_3$-OBP BHJ film is particularly interesting. It shows both large-scale aggregates of polymer (light regions) and fullerene-rich (dark regions) domains, contrast variations that cannot be explained as thickness fluctuations, with nanoscale phase separation that

dx.doi.org/10.1021/ja305875u | J. Am. Chem. Soc. 2012, 134, 15869−15879

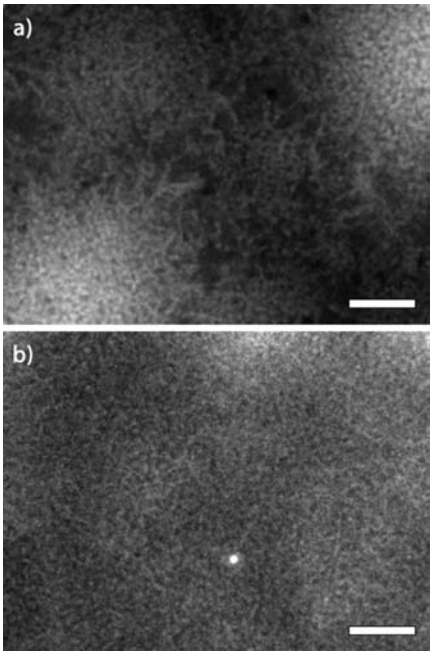

Figure 4. HAADF-STEM of solar cells comprised of: (a) P3HS:$(C_3H_7)_3$-OBP and (b) P3HS:$(C_6H_{13})_3$-OBP solar cell annealed at 150 °C for 10 min. The scale bar represents a distance of 200 nm. The bright spot in the center of (b) is an artifact from focusing the electron beam prior to imaging. The intensity of (a) is scaled −45% to +100% of the mean value and (b) is scaled ±45% of the mean value.

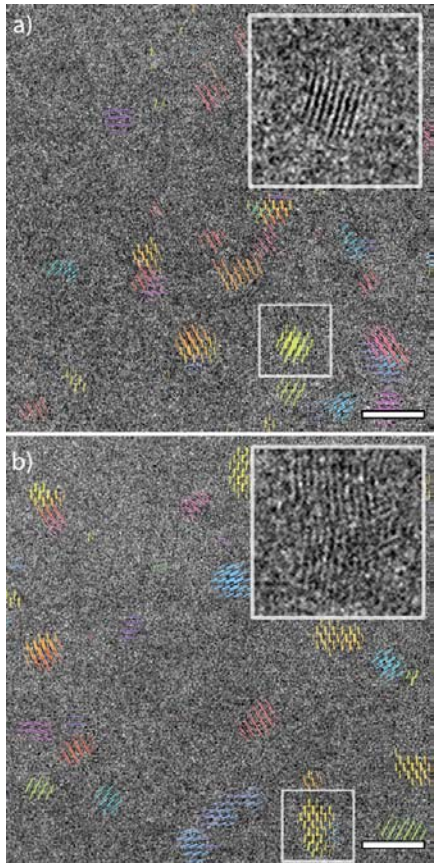

Figure 5. HRTEM images of P3HS BHJ blends. Regions showing lattice planes corresponding the alkyl stacking of P3HS ($d \sim 1.6$ nm) have been overlaid with tick marks drawn parallel to the lattice planes, and the width of the lines has been set proportional to the local intensity. The color of the lines has been set according to the direction to improve the visual contrast. P3HS:$(C_3H_7)_3$-OBP and P3HS:$(C_6H_{13})_3$-OBP are shown in (a,b), respectively. The scale bar represents a distance of 20 nm. The films show large-scale aggregates of polymer, and the crystals are most commonly found within these regions.

suggests a percolated network. The nanoscale network appears more developed relative to the bilayer experiments and is consistent with an active layer that contains a larger volume fraction of fullerene-rich domains. The surrounding enriched $(C_3H_7)_3$-OBP phase is likely a consequence of the relatively low miscibility of $(C_3H_7)_3$-OBP and P3HS, which leads to the precipitation of the fullerene-rich domains during the casting and annealing process. In the P3HS:$(C_6H_{13})_3$-OBP BHJ active layer, the miscibility of the fullerene in the polymer is increased, and the films become more homogeneous showing similar micro- and nanostructure to the bilayer experiments. These results are consistent with the theory that decreasing the polymer-fullerene miscibility can be utilized to increase the volume fraction of fullerene-rich domains.[51,52]

HRTEM was used to spatially resolve the in-plane oriented P3HS crystallites and found to be localized within the polymer-rich domains. While grazing incidence wide-angle X-ray scattering experiments have shown P3HS crystallites in P3HS and P3HS:PCBM BHJ films have the (100) alkyl chain stacking direction of the P3HS crystallites oriented predominately out of plane (i.e., edge-on) (ref 44 and Figure S7), in-plane alkyl stacking regions are observed throughout the film. For acquisition, the microscope was underfocused to image the 1.6 nm alkyl stacking peak of P3HS similar to previous studies of P3HT.[53−55] The insets of Figure 5a,b show typical images of P3HS:$(C_3H_5)_3$-OBP and P3HS:$(C_6H_{13})_3$-OBP BHJ films, respectively. False color overlays were produced by delineating lines of fixed length parallel to the visible lattice planes; the color was varied as a function of the relative in-plane lattice plane angle (Figure 5). The P3HS crystallites in both films were found to have slightly different dimensions. We note that the crystals were most concentrated within the polymer aggregates for the $(C_3H_7)_3$-OBP sample. In both blends, the fraction of the film covered by in-plane oriented crystallites is <10% of the total film area.

Qualitatively, the crystallite dimensions in the P3HS:$(C_3H_7)_3$-OBP BHJ appeared slightly smaller (roughly 10−30 nm) than those in P3HS:$(C_6H_{13})_3$-OBP (roughly 15−35 nm) suggesting a weak dependence on the miscibility. This conclusion is also supported by 2D wide-angle X-ray scattering in grazing-incidence geometry that probes the bulk ordering in the films (Figure S7). We do find it plausible that large weight fractions of fullerene within these blends will disrupt the formation of polymer crystallites.[56] We have not, however, observed this effect with the fullerenes here at the molar fractions used in this study. Furthermore, these data agree with a previously published report demonstrating that the mixed polymer-fullerene domains are comprised of disordered polymer and fullerene.[12,13] We note that the morphology, homogeneity, and crystallite size can be further manipulated with higher concentrations of the processing additive (discussed in the Supporting Information). HRTEM images indicate that P3HS crystallites are mainly located in the polymer-rich domains, implying that the mixed polymer and fullerene domains are predominately comprised of disordered

Table 1. Volume Fraction of Fullerene in the P3HS Bilayer Annealed at 150°C for 5 min (φ in P3HS), J_{sc}, V_{oc}, FF, PCE, R_s, and R_{sh} for P3HS:Fullerene Organic Solar Cells Fabricated with Equivalent Polymer-Fullerene Molar Ratios[a]

fullerene	φ in P3HS	J_{sc} (mA/cm^2)	V_{oc} (V)	FF	PCE (%)	R_s (Ω·cm^2)	R_{sh} (Ω·cm^2)
PCBM	0.73	6.9 ± 0.3	0.58	0.43	1.72	1.2	7×10^3
$(C_6H_{13})_3$-OBP	0.68	6.1 ± 0.3	0.64	0.43	1.67	4.0	30×10^3
$(C_3H_7)_3$-OBP	0.14	6.5 ± 0.1	0.61	0.61	2.45	1.8	20×10^3
$(C_2H_5)_3$-OBP	0.05	2.8 ± 0.1	0.64	0.48	0.87	2.0	10×10^3

[a]Typical variation in the V_{oc} and FF was <1%.

polymer and fullerene with the population of P3HS crystallites being weakly dependent to the polymer-fullerene miscibilities.

Linking the Polymer-Fullerene Miscibility to the Power Conversion Efficiency. BHJ solar cells comprised of P3HS and PCBM, $(C_2H_5)_3$-OBP, $(C_3H_7)_3$-OBP, or $(C_6H_{13})_3$-OBP were fabricated to correlate the polymer-fullerene miscibility and BHJ microstructures described above to the PCE. We found that for P3HS, the solar cells with the most efficient charge collection were fabricated with $(C_3H_7)_3$-OBP, a fullerene that is ~80% less miscible in P3HS relative to PCBM (φ_{C3H7} = 0.14 vs φ_{PCBM} = 0.73 measured at 150 °C). In order to draw these conclusions, the active layer thickness, processing conditions, and polymer-fullerene molar ratios (equivalent to a 1:0.7 weight ratio for P3HT:PCBM) were held constant for all devices. Note that the polymer-fullerene blend ratio is likely one of the factors that control the active layer microstructure; in this study, the blend ratio was held constant in order to highlight the impact of miscibility on the charge collection efficiency and PCE. All devices reported were fabricated with 1.5% vol 1-chloronaphthalene (CN) additive[57] and were annealed at 150 °C for 10 min. In each case, the P3HS:fullerene solar cells exhibited values <4 Ω·cm^2 for the series resistance (R_s) (estimated from the slope of the dark $J-V$ curve at 1.5 V) and values >10^4 Ω·cm^2 for the shunt resistances (R_{sh}) (estimated from the slope of the dark $J-V$ curve measured at −0.5 V), indicating classic dark diode behavior (additional device characteristics and dark and light $J-V$ curves found in Table 1 and Figure S8). Tuning the alkyl chain length of the 1,4-fullerene derivatives was found to have little impact on the measured V_{oc}, nominally 0.62 V. These findings imply that the structure of the different fullerenes used in this study has little effect on the frontier molecular orbital levels, a conclusion that is also supported by cyclic voltammograms (Figure S9).

First, we compare BHJs of P3HS:PCBM and P3HS:$(C_6H_{13})_3$-OBP which are films that comprise fullerenes of dissimilar structures but similar polymer-fullerene miscibilities. This comparison allows us to distinguish between contributions from either the fullerene structure or the polymer-fullerene miscibilities to the solar cell characteristics. It was found that the J_{sc} for P3HS:PCBM and P3HS:$(C_6H_{13})_3$-OBP was ~6.5 mA/cm^2 and within the typical variance observed for devices. Note that the lower J_{sc} relative to P3HT results in part from the reduced absorption coefficient in P3HS (Figure S13). Correcting for this decreased absorption coefficient (i.e., by normalizing the measured J_{sc} of the P3HS:PCBM solar cells by the integrated area of the absorption coefficient for the P3HS:PCBM and P3HT:PCBM active layers) yielded normalized values for the J_{sc} of P3HS:PCBM solar cells within 10% of values typically observed for P3HT:PCBM (i.e., ~9.0 mA/cm^2). Furthermore, as indicated by cyclic voltammetry, the value for the lowest unoccupied molecular orbital (LUMO) of the 1,4 fullerene adducts was ~0.1 eV higher than PCBM, which results in a slightly larger value for the V_{oc} in the devices comprised of P3HS:$(C_6H_{13})_3$-OBP (0.64 V) compared to P3HS:PCBM (0.58 V). Additionally, it was found that the FF of the P3HS:$(C_6H_{13})_3$-OBP devices was similar to the P3HS:PCBM devices, nominally 43%. These results reveal that BHJs with fullerene having dissimilar structures yet similar miscibility can yield solar cells with nearly identical characteristics suggesting that the polymer-fullerene miscibility is an important parameter for the final PCE.

As demonstrated above, decreasing the miscibility of the fullerene component in the P3HS increases the volume fraction of fullerene-rich domains, which should increase the charge collection efficiency. To investigate this, solar cells were fabricated with P3HS:$(C_3H_7)_3$-OBP and compared to those fabricated from P3HS:$(C_6H_{13})_3$-OBP. Decreasing the polymer-fullerene miscibility from φ_{C6H13} = 0.68 to φ_{C3H7} = 0.14 (concentrations measured from the volume fraction of miscible fullerene measured after annealing at 150 °C as described above) had little influence on the J_{sc}, nominally 6.5 mA/cm^2 (Figure 6b and Table 1). Most importantly, it was found that

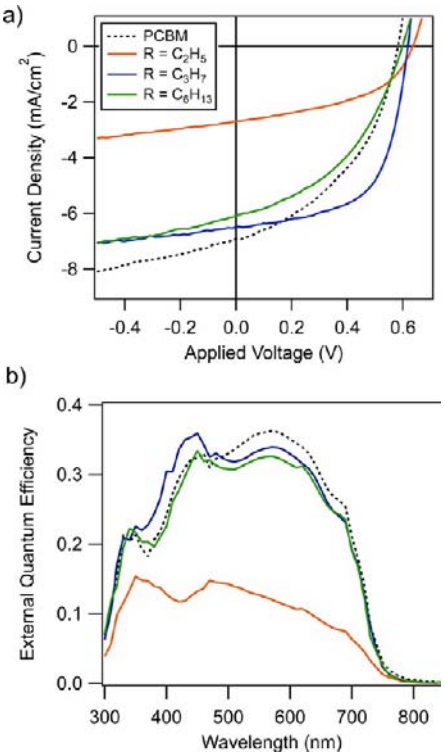

Figure 6. (a) $C-V$ measurements under AM 1.5G illumination and (b) EQE spectrum for solar cells fabricated with a combination of P3HS and PCBM (dotted black), $(C_2H_5)_3$-OBP (solid orange), $(C_3H_7)_3$-OBP (solid blue), or $(C_6H_{13})_3$-OBP (solid green). The solar cell had similar active layer thicknesses (~90 nm) and molar ratios of polymer:fullerene equivalent to a 1:0.7 weight ratio of P3HT:PCBM.

dx.doi.org/10.1021/ja305875u | J. Am. Chem. Soc. 2012, 134, 15869−15879

the bias-dependent charge collection efficiency or fill factor (FF) increased as the polymer-fullerene miscibility was decreased. The FF can be understood as the voltage-dependent probability for free charge carrier collection or $P_C(V)$.[58] Assuming that the device can be modeled as a current generator and diode in parallel, the net current measured (J_G) under an applied voltage (V) and charge generation rate (G_{PH}) can be represented as follows:

$$J_G = J_{dark}(V) - eP_C(V)G_{PH}$$

where J_{dark} is the voltage-dependent dark current and P_C is the probability for charge collection at an applied bias and is proportional to the FF. Note that the photocurrent density (J_{PH}) is equal to $eP_C(V)G_{PH}$. An ideal solar cell would exhibit a bias-independent value for P_C equal to unity. Decreasing values for P_C indicate that an increased fraction of the generated free charge carriers recombines before collection and directly relates to the FF. It was found that the P_C or FF of the P3HS:fullerene solar cells improved as the polymer-fullerene miscibility was decreased from φ_{C6H13} = 0.68 to φ_{C3H7} = 0.14 (43 to 61%, respectively). To our knowledge, the 61% FF for the P3HS:$(C_3H_7)_3$-OBP devices is the highest reported value for P3HS:fullerene BHJs. From the evidence presented above, it is clear that the increase in the charge collection efficiency is due to the increase in the volume fraction of fullerene-rich domains. With P3HS, it was necessary to decrease the polymer-fullerene miscibility, which increases the volume fraction of fullerene-rich domains and thus improves the charge carrier collection efficiency. Thus, the polymer-fullerene miscibility can be utilized to tune the volume fraction of rich and mixed polymer and fullerene domains, which, in this case, improves the PCE.

As the fullerene miscibility in the P3HS was decreased from φ_{C3H7} = 0.14 to φ_{C2H5} = 0.05, it was found that the current generated decreased by more than 50%, from ~6.5 to ~3.0 mA/cm^2, respectively. These differences in the J_{sc} are confirmed by a decrease in the external quantum efficiency (EQE), from a peak value of 36 to 15% for the devices comprised of P3HS and $(C_3H_7)_3$-OBP and $(C_2H_5)_3$-OBP, respectively (Figure 6b). As the miscibility of the fullerene in P3HS decreases, there is an increase in the volume fraction of fullerene-rich domains. In this case, a large fraction of the fullerene exists as pure fullerene crystallites, as indicated by XRD (Figure S7) and the HAADF STEM bilayer images. It is likely that the J_{sc} is limited by the low interfacial area between the polymer- and fullerene-rich domains, indicating that increasing the surface area between the polymer and fullerene components (achieved by increasing the polymer-fullerene miscibility) improves charge generation.

The key finding is that decreasing the polymer-fullerene miscibility (i.e., decreasing fraction of mixed polymer-fullerene domains) can be used to increase the charge collection efficiency within P3HS-fullerene BHJ organic solar cells. However, since current generation is proportional to the surface area between the polymer and fullerene components, increasing the volume fraction of fullerene- and polymer-rich domains will limit the current generated in some cases. As a balance, there must therefore be an ideal microstructure for polymer-fullerene solar cells, which will maximize both mobile charge generation and collection.

Linking the Polymer-Fullerene Miscibility to the Recombination Mechanism. To examine a mechanism for recombination in these devices, we used the Hecht expression to relate the charge collection efficiency (or charge carrier trapping probability) to the polymer-fullerene miscibility. In the Hecht expression:

$$\frac{Q}{Q_0} = \frac{\mu\tau(V_s - V)}{dd'}\left\{1 - \exp\left[-\frac{dd'}{\mu\tau(V_s - V)}\right]\right\}$$

where d is the sample thickness and d' is the collection length.[59] Since comparisons are being made between cells of similar thicknesses and absorption profiles, it is safe to assume that the collection length is similar and is about half the thickness of the cell (45 nm). We also expect that the free charge carrier generation rate is relatively insensitive to fullerene structure due to the well-known ultrafast electron transfer between polymers and fullerenes.[60,61] Q/Q_0 is defined as the fraction of generated free charge carriers collected by the electrodes relative to the total amount of charge generated (i.e., Q_0 = photocurrent measured at −1 V (J_{SAT})). V_S is defined as the voltage at which the photocurrent ($J_{PH} = J_{light} - J_{dark}$) is equal to zero, and V is the voltage applied across the electrodes. The μ is the average free charge carrier mobility, and τ is the average free charge carrier lifetime. It is generally assumed that the polymer-rich phase is responsible for hole transport, and the fullerene-rich phase is responsible for the electron transport, thus the product of $\mu\tau$ is a property of both materials and determines the voltage-dependent free charge carrier collection. Note that larger values for the mobility-lifetime product ($\mu\tau/dd'$) correspond to a higher probability for free charge carrier collection (i.e., larger value for the P_C and FF). In all cases, the J_{sc} of the devices was found to be proportional to the light intensity (Figure S10). All values for the mobility-lifetime product agreed well with the photocurrent−voltage data with illumination intensities ranging over a factor of ~25. Additional information can be found in the Supporting Information.

It was found that solar cells fabricated with P3HS and $(C_3H_7)_3$-OBP yielded the highest mobility-lifetime product over all light intensities examined. Figure 7 represents the mobility-lifetime product as a function of light intensity at room temperature. It was found that the P3HS:$(C_3H_7)_3$-OBP solar

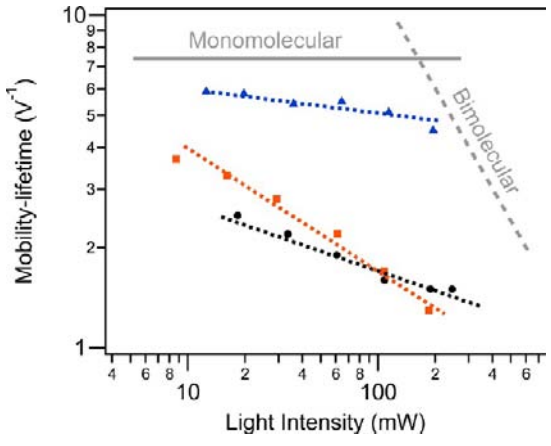

Figure 7. Mobility lifetime product ($\mu\tau/dd'$) of a P3HS:fullerene solar cells obtained from the fits of the photocurrent−voltage data as a function of light intensity: PCBM (black circles), $(C_3H_7)_3$-OBP (blue triangles), and $(C_6H_{13})_3$-OBP (orange squares). The expected qualitative trends for monomolecular (solid) and bimolecular (dashed) recombination are annotated on the graph. The colored dashed lines correspond to a fit of the mobility-lifetime product as a function of light intensity and correspond to a slope of 0.21, 0.34, and 0.09 for PCBM, $(C_6H_{13})_3$-OBP, and $(C_3H_7)_3$-OBP, respectively.

dx.doi.org/10.1021/ja305875u | J. Am. Chem. Soc. 2012, 134, 15869−15879

cells (80% less miscible with P3HS relative to PCBM, φ_{C3H7} = 0.14) have the highest value for the FF, correlating to the highest value for the mobility-lifetime product of 5.1 V^{-1} at 1 sun. Additionally, it was found that the P3HS:PCBM and P3HS:$(C_6H_{13})_3$-OBP, active layers with similar polymer-fullerene miscibilities (φ_{C6H13} = 0.68 and φ_{PCBM} = 0.73 measured at 150 °C) and microstructures also gave very similar values for the FF (~43%) as well as the mobility-lifetime product of 1.6 V^{-1} and 1.7 V^{-1} respectively at 1 sun illumination. Thus, it was observed that the mobility-lifetime product improved by a factor of 3 by decreasing the polymer-fullerene miscibility in a P3HS:fullerene BHJ solar cell. Again, these results indicate that decreasing the miscibility of the fullerene in P3HS increases the volume fraction of fullerene-rich domains leading to more efficient charge collection pathways, which is revealed by the increase in mobility-lifetime product observed in the P3HS:$(C_3H_7)_3$-OBP solar cells at all measured charge densities.

Additionally, the light-intensity dependence of the mobility-lifetime product reveals that the P3HS:$(C_3H_7)_3$-OBP BHJ solar cells had the lowest probability for recombination over the whole range of illumination. One expects the slope of the mobility-lifetime product vs carrier concentration (light intensity) to increase in magnitude if bimolecular recombination, or at least an apparent mechanism that is higher than simple monomolecular kinetics,[62] is a dominant mechanism. Here we do not have a direct measure of the charge carrier concentration or the level of doping of the P3HS, as has been suggested to be important for P3HT,[62] but we do find a connection between the light dependence and the miscibility. As the number of trap states increases, we expect to observe changes in the recombination kinetics[63] and the mobility-lifetime product should have an increased dependence on light intensity (i.e., steeper slope). It was found that the dependence of the mobility-lifetime product on the light intensity (i.e., exponent) was 0.09, 0.21, and 0.34 for the P3HS:fullerene solar cells fabricated from the $(C_3H_7)_3$-OBP, PCBM, and $(C_6H_{13})_3$-OBP, respectively (Figure 7). These data indicate that decreasing the polymer-fullerene miscibility (i.e., increasing the volume fraction of fullerene-rich domains) likely decreases the density of charge traps, which leads to the more efficient charge collection observed in the P3HS:$(C_3H_7)_3$-OBP solar cells. The direct correlation between the trap density and the polymer-fullerene miscibility suggests that there is a higher density of charge traps in the polymer-fullerene mixed domains. Given the similar active layer microstructures and polymer-fullerene miscibilities, it was interesting that the slope of the mobility-lifetime product with respect to light intensity in solar cells comprising P3HS and either PCBM or $(C_6H_{13})_3$-OBP was different. It is likely that this difference arises from dissimilar charge trap densities and relative trap depths. Again, the results indicate that tuning the polymer-fullerene miscibility is a viable and potentially powerful strategy for improving charge collection within polymer-fullerene organic solar cells and thus the PCE of an organic solar cell.

CONCLUSION

The design of a series of fullerene derivatives allowed the polymer-fullerene miscibility to be rationally varied and permitted the temperature-dependent polymer-fullerene miscibility and microstructure to be quantified after heat treatment using a model bilayer structure. A direct correlation between the fullerene alkyl chain length, polymer-fullerene miscibility, and the resulting bilayer microstructure was clearly observed with a decrease in the fullerene alkyl chain length leading to a decrease in polymer-fullerene miscibility and concomitant increase in the relative volume fraction of polymer- and fullerene-rich domains in the annealed bilayer films. Additionally, BHJ samples showed a similar dependence of the microstructure on the polymer-fullerene miscibility (i.e., increasing the volume fraction of polymer- and fullerene-rich domains) within the BHJ films with little change in the total population of P3HS crystallites. Solar cell characteristics revealed that decreasing the polymer-fullerene miscibility in P3HS:fullerene solar cells (relative to PCBM) increases the charge collection efficiency, which reduces the probability for recombination by more than a factor of 3. A key finding of this study is that the reliance on PCBM in OPV devices does not permit the full range of microstructures of polymer-fullerene BHJs to be accessed. In turn, this choice handicaps important strategies for improving charge collection efficiency and PCE for polymer-fullerene BHJ solar cells.

Our results suggest the potential utility of using the miscibility of the electron-donating and -accepting materials as a metric for screening new material combinations for high-performance OPVs. The miscibility was shown to be a readily measurable quantity, which can then be linked to the BHJ microstructure and the charge collection efficiency and can provide an added degree of control over the formation of the BHJ. Measuring the polymer and fullerene miscibility therefore represents a simple method for screening specific material combinations in order to maximize both the charge generation and the efficiency of free charge carrier collection.

ASSOCIATED CONTENT

Supporting Information

Additional DSIMS profiles, UV−vis spectrum, TEM images, and solar cell characteristics. This material is available free of charge via the Internet at http://pubs.acs.org.

AUTHOR INFORMATION

Corresponding Author

mchabinyc@engineering.ucsb.edu

Notes

The authors declare no competing financial interest.

ACKNOWLEDGMENTS

We thank the NSF SOLAR and NSF International Collaboration in Chemistry programs for partial support of this work (CHE-1035292 and 1026664, C.J.H. and M.L.C.) and the EPSRC (international collaboration in chemistry EP/I002936/1). N.D.T. acknowledges support from the ConvEne IGERT program (NSF-DGE 0801627) and NSF Graduate Research Fellowship. C.J.T. and A.J.H. would like to acknowledge NSF-DMR 0856060 for providing support for the TEM imaging. Portions of this work were carried out using the MRL Central Facilities, which are supported by the MRSEC Program of the NSF under award no. DMR-1121053; a member of the NSF funded Materials Research Facilities Network (www.mrfn.org). The authors would like to thank Dr. Thomas Mates for assistance with the DSIMS measurements. Additionally, the authors thank Edward Kramer, Dago de Leeuw, Natalie Stingelin, and Paul Smith for their insightful discussions.

REFERENCES

(1) Green, M. A.; Emery, K.; Hishikawa, Y.; Warta, W.; Dunlop, E. D. *Prog. Photovoltaics* **2012**, *20* (1), 12−20.
(2) Li, G.; Zhu, R.; Yang, Y. *Nat. Photonics* **2012**, *6* (3), 153−161.
(3) Woo, C. H.; Beaujuge, P. M.; Holcombe, T. W.; Lee, O. P.; Frechet, J. M. J. *J. Am. Chem. Soc.* **2010**, *132* (44), 15547−15549.
(4) Ku, S.-Y.; Liman, C. D.; Burke, D. J.; Treat, N. D.; Cochran, J. E.; Amir, E.; Perez, L. A.; Chabinyc, M. L.; Hawker, C. J. *Macromolecules* **2011**, *44* (24), 9533−9538.
(5) Chu, T.-Y.; Lu, J.; Beaupre, S.; Zhang, Y.; Pouliot, J.-R.; Wakim, S.; Zhou, J.; Leclerc, M.; Li, Z.; Ding, J.; Tao, Y. *J. Am. Chem. Soc.* **2011**, *133* (12), 4250−4253.
(6) Liang, Y. Y.; Xu, Z.; Xia, J. B.; Tsai, S. T.; Wu, Y.; Li, G.; Ray, C.; Yu, L. P. *Adv. Mater.* **2010**, *22* (20), E135−E138.
(7) Amb, C. M.; Chen, S.; Graham, K. R.; Subbiah, J.; Small, C. E.; So, F.; Reynolds, J. R. *J. Am. Chem. Soc.* **2011**, *133* (26), 10062−10065.
(8) Wang, E.; Ma, Z.; Zhang, Z.; Vandewal, K.; Henriksson, P.; Inganäs, O.; Zhang, F.; Andersson, M. R. *J. Am. Chem. Soc.* **2011**, *133* (36), 14244−14247.
(9) Peet, J.; Kim, J. Y.; Coates, N. E.; Ma, W. L.; Moses, D.; Heeger, A. J.; Bazan, G. C. *Nat. Mater.* **2007**, *6* (7), 497−500.
(10) Chen, H. Y.; Hou, J. H.; Zhang, S. Q.; Liang, Y. Y.; Yang, G. W.; Yang, Y.; Yu, L. P.; Wu, Y.; Li, G. *Nat. Photonics* **2009**, *3* (11), 649−653.
(11) Lee, J. K.; Ma, W. L.; Brabec, C. J.; Yuen, J.; Moon, J. S.; Kim, J. Y.; Lee, K.; Bazan, G. C.; Heeger, A. J. *J. Am. Chem. Soc.* **2008**, *130* (11), 3619−3623.
(12) Treat, N. D.; Brady, M. A.; Smith, G.; Toney, M. F.; Kramer, E. J.; Hawker, C. J.; Chabinyc, M. L. *Adv. Energy Mater.* **2011**, *1* (1), 82−89.
(13) Treat, N. D.; Shuttle, C. G.; Toney, M. F.; Hawker, C. J.; Chabinyc, M. L. *J. Mater. Chem.* **2011**, *21* (39), 15224−15231.
(14) Watts, B.; Belcher, W. J.; Thomsen, L.; Ade, H.; Dastoor, P. C. *Macromolecules* **2009**, *42* (21), 8392−8397.
(15) Collins, B. A.; Tumbleston, J. R.; Ade, H. *J. Phys. Chem. Lett.* **2011**, *2* (24), 3135−3145.
(16) Agostinelli, T.; Lilliu, S.; Labram, J. G.; Campoy-Quiles, M.; Hampton, M.; Pires, E.; Rawle, J.; Bikondoa, O.; Bradley, D. D. C.; Anthopoulos, T. D.; Nelson, J.; Macdonald, J. E. *Adv. Funct. Mater.* **2011**, *21* (9), 1701−1708.
(17) Chen, D.; Nakahara, A.; Wei, D.; Nordlund, D.; Russell, T. P. *Nano Lett.* **2011**, *11* (2), 561−567.
(18) Yang, X. N.; Loos, J.; Veenstra, S. C.; Verhees, W. J. H.; Wienk, M. M.; Kroon, J. M.; Michels, M. A. J.; Janssen, R. A. J. *Nano Lett.* **2005**, *5* (4), 579−583.
(19) Wang, T.; Pearson, A. J.; Lidzey, D. G.; Jones, R. A. L. *Adv. Funct. Mater.* **2011**, *21* (8), 1383−1390.
(20) Miller, N. C.; Gysel, R.; Miller, C. E.; Verploegen, E.; Beiley, Z.; Heeney, M.; McCulloch, I.; Bao, Z.; Toney, M. F.; McGehee, M. D. *J. Polym. Sci., Part B: Polym. Phys.* **2011**, *49* (7), 499−503.
(21) Beaujuge, P. M.; Frechet, J. M. J. *J. Am. Chem. Soc.* **2011**, *133* (50), 20009−20029.
(22) Fei, Z.; Ashraf, R. S.; Huang, Z.; Smith, J.; Kline, R. J.; D'Angelo, P.; Anthopoulos, T. D.; Durrant, J. R.; McCulloch, I.; Heeney, M. *Chem. Commun.* **2012**, *48* (24), 2955−2957.
(23) Kozub, D. R.; Vakhshouri, K.; Orme, L. M.; Wang, C.; Hexemer, A.; Gomez, E. D. *Macromolecules* **2011**, *44* (14), 5722−5726.
(24) Zhou, H.; Yang, L.; Xiao, S.; Liu, S.; You, W. *Macromolecules* **2009**, *43* (2), 811−820.
(25) Nguyen, L. H.; Hoppe, H.; Erb, T.; Günes, S.; Gobsch, G.; Sariciftci, N. S. *Adv. Funct. Mater.* **2007**, *17* (7), 1071−1078.
(26) Piliego, C.; Holcombe, T. W.; Douglas, J. D.; Woo, C. H.; Beaujuge, P. M.; Frechet, J. M. J. *J. Am. Chem. Soc.* **2010**, *132* (22), 7595−7597.
(27) Coffin, R. C.; Peet, J.; Rogers, J.; Bazan, G. C. *Nat. Chem.* **2009**, *1* (8), 657−661.
(28) Liang, Y.; Yu, L. *Acc. Chem. Res.* **2010**, *43* (9), 1227−1236.
(29) McCulloch, I.; Ashraf, R. S.; Biniek, L.; Bronstein, H.; Combe, C.; Donaghey, J. E.; James, D. I.; Nielsen, C. B.; Schroeder, B. C.; Zhang, W. *Acc. Chem. Res.* **2012**, *45* (5), 714−722.
(30) Yiu, A. T.; Beaujuge, P. M.; Lee, O. P.; Woo, C. H.; Toney, M. F.; Frechet, J. M. J. *J. Am. Chem. Soc.* **2012**, *134* (4), 2180−2185.
(31) Xia, R.; Al-Hashimi, M.; Tsoi, W. C.; Heeney, M.; Bradley, D. D. C.; Nelson, J. *Sol. Energy Mater. Sol. Cells* **2012**, *96* (1), 112−116.
(32) Troshin, P. A.; Hoppe, H.; Renz, J.; Egginger, M.; Mayorova, J. Y.; Goryochev, A. E.; Peregudov, A. S.; Lyubovskaya, R. N.; Gobsch, G.; Sariciftci, N. S.; Razumov, V. F. *Adv. Funct. Mater.* **2009**, *19* (5), 779−788.
(33) He, Y.; Chen, H.-Y.; Hou, J.; Li, Y. *J. Am. Chem. Soc.* **2010**, *132* (4), 1377−1382.
(34) Lenes, M.; Wetzelaer, G.-J. A. H.; Kooistra, F. B.; Veenstra, S. C.; Hummelen, J. C.; Blom, P. W. M. *Adv. Mater.* **2008**, *20* (11), 2116−2119.
(35) Shuttle, C. G.; Treat, N. D.; Fan, J.; Varotto, A.; Hawker, C. J.; Wudl, F.; Chabinyc, M. L. *J. Polym. Sci., Part B: Polym. Phys.* **2012**, *50* (3), 174−179.
(36) Varotto, A.; Treat, N. D.; Jo, J.; Shuttle, C. G.; Batara, N. A.; Brunetti, F. G.; Seo, J. H.; Chabinyc, M. L.; Hawker, C. J.; Heeger, A. J.; Wudl, F. *Angew. Chem., Int. Ed.* **2011**, *50* (22), 5166−5169.
(37) Niinomi, T.; Matsuo, Y.; Hashiguchi, M.; Sato, Y.; Nakamura, E. *J. Mater. Chem.* **2009**, *19* (32), 5804−5811.
(38) Li, C.-Z.; Chien, S.-C.; Yip, H.-L.; Chueh, C.-C.; Chen, F.-C.; Matsuo, Y.; Nakamura, E.; Jen, A. K. Y. *Chem. Commun.* **2011**, *47* (36), 10082−10084.
(39) Kastner, C.; Susarova, D. K.; Jadhav, R.; Ulbricht, C.; Egbe, D. A. M.; Rathgeber, S.; Troshin, P.; Hoppe, H. *J. Mater. Chem.* **2012**, *31* (22), 15987−15997.
(40) Zhang, Y.; Yip, H.-L.; Acton, O.; Hau, S. K.; Huang, F.; Jen, A. K. Y. *Chem. Mater.* **2009**, *21* (13), 2598−2600.
(41) Ballantyne, A. M.; Ferenczi, T. A. M.; Campoy-Quiles, M.; Clarke, T. M.; Maurano, A.; Wong, K. H.; Zhang, W.; Stingelin-Stutzmann, N.; Kim, J.-S.; Bradley, D. D. C.; Durrant, J. R.; McCulloch, I.; Heeney, M.; Nelson, J.; Tierney, S.; Duffy, W.; Mueller, C.; Smith, P. *Macromolecules* **2010**, *43* (3), 1169−1174.
(42) Hernandez, S.; Moreno, I.; SanMartin, R.; Gomez, G.; Teresa Herrero, M.; Dominguez, E. *J. Org. Chem.* **2010**, *75* (2), 434−441.
(43) Sun, Y.; Welch, G. C.; Leong, W. L.; Takacs, C. J.; Bazan, G. C.; Heeger, A. J. *Nat. Mater.* **2012**, *11* (1), 44−48.
(44) Lilliu, S.; Agostinelli, T.; Verploegen, E.; Pires, E.; Hampton, M.; Al-Hashimi, M.; Heeney, M. J.; Toney, M. F.; Nelson, J.; Macdonald, J. E. *Macromol. Rapid Commun.* **2011**, *32* (18), 1454−1460.
(45) Ballantyne, A. M.; Chen, L.; Nelson, J.; Bradley, D. D. C.; Astuti, Y.; Maurano, A.; Shuttle, C. G.; Durrant, J. R.; Heeney, M.; Duffy, W.; McCulloch, I. *Adv. Mater.* **2007**, *19* (24), 4544−4547.
(46) Heeney, M.; Zhang, W.; Crouch, D. J.; Chabinyc, M. L.; Gordeyev, S.; Hamilton, R.; Higgins, S. J.; McCulloch, I.; Skabara, P. J.; Sparrowe, D.; Tierney, S. *Chem. Commun.* **2007**, *47*, 5061−5063.
(47) Klein, M. F. G.; Pfaff, M.; Mueller, E.; Czolk, J.; Reinhard, M.; Valouch, S.; Lemmer, U.; Colsmann, A.; Gerthsen, D. *J. Polym. Sci., Part B: Polym. Phys.* **2012**, *50* (3), 198−206.
(48) Hollinger, J.; Jahnke, A. A.; Coombs, N.; Seferos, D. S. *J. Am. Chem. Soc.* **2010**, *132* (25), 8546−8547.
(49) Reimer, L.; Kohl, H. I. *Springer Series in Optical Sciences*, 5th ed.; Springer: New York, 2008; Vol. *36*.
(50) Rez, D.; Rez, P.; Grant, I. *Acta Crystallogr., Sect. A* **1994**, *50*, 481−497.
(51) Labram, J. G.; Kirkpatrick, J.; Bradley, D. D. C.; Anthopoulos, T. D. *Phys. Rev. B* **2011**, *84* (7), 075344.
(52) Vakhshouri, K.; Kozub, D. R.; Wang, C.; Salleo, A.; Gomez, E. D. *Phys. Rev. Lett.* **2012**, *108* (2), 026601.
(53) Lovinger, A. J.; Katz, H. E.; Dodabalapur, A. *Chem. Mater.* **1998**, *10* (11), 3275−3277.
(54) Brinkmann, M.; Rannou, P. *Macromolecules* **2009**, *42* (4), 1125−1130.
(55) Drummy, L. F.; Davis, R. J.; Moore, D. L.; Durstock, M.; Vaia, R. A.; Hsu, J. W. P. *Chem. Mater.* **2011**, *23* (3), 907−912.

(56) Verploegen, E.; Mondal, R.; Bettinger, C. J.; Sok, S.; Toney, M. F.; Bao, Z. A. *Adv. Funct. Mater.* **2010**, *20* (20), 3519−3529.
(57) Chen, F.-C.; Tseng, H.-C.; Ko, C.-J. *Appl. Phys. Lett.* **2008**, *92* (10), 103316.
(58) Street, R. A.; Schoendorf, M. *Phys. Rev. B* **2010**, *81* (20), 205307.
(59) Hecht, K. *Z. Phys. A: Hadrons Nucl.* **1932**, *77* (3), 235−245.
(60) Sariciftci, N. S.; Smilowitz, L.; Heeger, A. J.; Wudl, F. *Science* **1992**, *258* (5087), 1474−1476.
(61) Clarke, T. M.; Durrant, J. R. *Chem. Rev.* **2010**, *110* (11), 6736−6767.
(62) Chuttle, C. G.; Treat, N. D.; Douglas, J. D.; Frechet, J. M. J.; Chabinyc, M. L. *Adv. Energy Mater.* **2012**, *2* (1), 111−119.
(63) Maurano, A.; Shuttle, C. G.; Hamilton, R.; Ballantyne, A. M.; Nelson, J.; Zhang, W.; Heeney, M.; Durrant, J. R. *J. Phys. Chem. C* **2011**, *115*, 5947−5957.